Shen WA, Zhu S and Xu YL (2012) An experimental study on self-powered vibration control and monitoring system using electromagnetic TMD and wireless sensors. *Sensors and Actuators A: Physical*. 180: 166-176.

An Experimental Study on Self-powered Vibration Control and Monitoring System using Electromagnetic TMD and Wireless Sensors

Wen-ai Shen, Songye Zhu* and You-lin Xu

Department of Civil and Structural Engineering, The Hong Kong Polytechnic University, Kowloon, Hong Kong

*Corresponding author: ceszhu@polyu.edu.hk

ABSTRACT

This paper proposed and validated a self-powered vibration control and monitoring (SVCM) system which consists of a pendulum-type tuned mass damper (TMD), a rotary electromagnetic (EM) device, an energy harvesting circuit (EHC) and a wireless smart sensor (WSS). As the key element in the system, the regenerative electromagnetic TMD (EMTMD) is able to convert vibration energy of structures to electrical energy, and thus plays dual functions, namely, vibration mitigation and energy harvesting. With the aid of EHC, the electrical energy can be further stored and used to power WSS that closely monitor structural vibration responses. The feasibility of the proposed SVCM system was validated via shaking table tests, in which a single-degree-of-freedom (SDOF) structural model equipped with the SVCM system was tested under random excitations. The functionality of the SVCM system was discussed with regard to the vibration control, energy harvesting and vibration monitoring performance. The experimental results revealed that the proposed regenerative EMTMD device can provide regenerative and economical power to WSS. The harvested power reaches about 312.4 mW under random ground motions with root-mean-square (RMS) acceleration equal to 0.05g. Meanwhile, the comparison shows that the peak magnitude of the frequency response function of structural displacement is reduced by 10 dB with the aid of the EMTMD. This study demonstrates that the SVCM system provides a novel and promising solution to the power supply problem associated with wireless sensing technology, and will stimulate the integration of vibration control and monitoring system.

INTRODUCTION

Emerging wireless sensor technology has seen growing applications in the health monitoring of mechanical, aerospace and civil structures. The limited lifespan of batteries has motivated researchers to seek alternative and reliable power supply to wireless sensing nodes from ambient light, wind, heat, strain, radio and vibrations [1],[2],[3]. In particular, vibration-based energy harvesting techniques were developed based on various different transduction mechanisms, e.g. electromagnetic induction[4-6], piezoelectricity[7-10], electrostatic generation [11] dielectric elastomers [12] and so on. Many vibration-based energy harvesting devices are essentially micro or small resonant structures (e.g. a beam with a proof mass). The output power of such micro devices usually ranges from μWs to mWs[13], whereas the typical power consumption of a

wireless smart sensor (WSS) is from tens of to hundreds of mWs [1, 14]. The existing gap in terms of power implies the necessity of developing vibration-based energy harvesting devices with relatively large size and output power in order to meet the power requirement of existing wireless sensors. On the other hand, vibration is ubiquitous in civil engineering structures. In fact, many flexible and lightly damped civil structures (such as high-rise buildings, long-span bridges, stay cables, etc.) are vulnerable to excessive vibrations induced by traffics, wind, waves or earthquakes. Substantial researches have been done on structural vibration mitigation through energy dissipation strategy, in which various damping devices were successfully used, e.g. friction dampers, metallic yield dampers, buckling-restrained braces, viscous fluid dampers, visco-elastic dampers, tuned mass damper (TMD), electromagnetic (EM) dampers, magneto-rheological (MR) fluid dampers, and so on [15-17]. Among them, TMD, a resonant energy absorber, becomes an effective vibration control device seeing wide applications in civil and mechanical structures, e.g. in high-rise building, tall chimney, ships and aircraft engines[15, 18]. A recent well-known example is the pendulum-type TMD (730 tons) in Taipei 101 tower[19]. In conventional energy dissipation strategy, a great amount of vibration energy is converted to heat, and it is thus often associated with the self-heating of dampers.

In spite of the evidently complementary nature of damper system and wireless sensor system with regard to energy, surprisingly few attempts have been made so far to investigate the feasibility of taking advantage of the clean and renewable energy from damping devices to power wireless sensors, particularly in the area of civil engineering even though they co-exist in many newly built civil structures. This paper proposes a novel application of an integrated damper-sensor system, termed self-powered vibration control and monitoring (SVCM) system, in which EM devices function as vibration dampers and energy harvesters simultaneously, providing both counteraction damping forces to vibrating structures and power supply to WSS that closely monitor structural response. Such a new strategy is especially appealing to WSS that only need to work during vibrations induced by various excitations. An electromagnetic TMD (EMTMD) in connection with an energy harvesting circuit (EHC) plays a key role in the proposed SVCM system. A series of shaking table experiments were carried out for a proof of concept, in which a SDOF structure equipped with the proposed SVCM system was tested. The functionality of the SVCM system was discussed with regard to structural control, energy harvesting and vibration monitoring performance. The testing results successfully validate the feasibility of establishing an SVCM system based on EMTMD, WSS and EHC.

SVCM System Description

Configuration

Figure 1 illustrates a schematic of a structure equipped with a SVCM system. The SVCM system comprises a pendulum-type TMD, a rotary EM damper, an EHC and a WSS. A simple pendulum is a common form of TMD, which attaches an auxiliary mass to a primary structure through a pendulum and a damper. It is a resonant device oscillating at a similar frequency of the structure but with a phase shift, and it actually adds another degree-of-freedom (DOF) to the primary structure. The damping characteristic of the TMD is mainly contributed by a rotary EM damper in this study. It should be noted that according to Faraday's Law and Lorentz's Law, any permanent-magnet motors or generators, either DC or AC and either linear or rotary, can function as passive EM damper [20-23]. A gearbox is often needed to amplify the damping capacity and output power. The EMTMD could dissipate structural vibration energy and convert it to electrical energy, which is further harvested and stored by EHC and used to power one or more WSS nodes that closely monitor the dynamic response of the structure.

Experimental Setup

Shaking table tests of a single-story frame equipped with a SVCM system were carried out for a proof of concept [Figure 2]. The single-story steel frame represents a generic single-degree-of-freedom (SDOF) structure. Table 1 shows the dimensions, frequencies and damping ratios of the standalone steel frame without TMD and the mechanical properties of the pendulum-type EMTMD. Due to the light damping feature of the steel frame, its inherent damping ratio without TMD was enhanced to 0.95% by adding another oil damper to mimic real-world examples. The ratio of the TMD mass to the frame mass is 3.3%. According to [15], the optimal frequency and damping ratio can be calculated as 1.033 Hz and 11.07%. The measured frequency ratio and damping ratio shown in Table 1 are close to these optimal values. The damping characteristic of the TMD is mainly contributed by a three-phase rotary EM damper with a length of 94mm and a diameter of 78mm. It is composed of pairs of permanent magnets and coils, and its configuration is essentially the same as a conventional three-phase alternator. A gearbox with a ratio of 1:8 is used to enhance the rotational speed of the EM damper. As a result, it also magnifies the damping of the EMTMD n^2 times, where the gear box ratio $n = 8$.

A rechargeable Li-ions battery (capacity: 1840mAh, nominal voltage: 3.7V) was selected as the energy storage element. Compared with a supercapacitor, a rechargeable battery usually has more stable voltage during the charging process and smaller self-discharge rate. Among various rechargeable batteries (e.g. Li-ions, NiMH, NiCd, SLA, Li Polymer, etc), the Li-ions battery has relatively high power density [24]. Two EHCs described in the next section were tested individually in the shaking table experiments.

A WSS consisting of Imote2 wireless sensing platform [25]and a SHM-A multi-metric sensor board [26-28] was installed to measure the acceleration response of the frame with a sampling frequency of 100 Hz. The measurement range and sensitivity of the three-axis accelerometer on the SHM-A sensor board is ±2g and

0.66V/g [27]. Besides three-axis accelerometers, the SHM-A sensor board incorporates digital light, temperature and humidity sensors that were not utilized in this study. Voltage range between 3.7V to 4.7V is allowed by the Imote2 battery board [25], and thus it can be directly powered by the Li-ion battery. The power consumption of Imote2 with a SHM-A sensing board is about 204 mW in standby state, while it consumes about 625~865 mW in a 3-channel sensing mode.

In addition to the WSS, another wired sensing system was installed for a purpose of verification and evaluation of the SVCM system. More comprehensive responses were collected by KYOWA EDX-100A data acquisition system with a sampling frequency of 100Hz, including the accelerations of the shaking table and frame, the displacement of the shaking table, frame and the pendulum, the corresponding voltages and currents within the EHCs. In civil structures, harvesting energy from structural ambient vibrations induced by traffic, pedestrians, wind, waves and ground motions is of interesting. These ambient vibrations are typically random with low frequencies. Random vibrations are widely used to represent generic ambient vibration in energy harvesting study [29]. Therefore, a series of shaking table tests were carried out under random excitations with relatively low frequency components (a band-limited white noise with a bandwidth of 0.5-10 Hz) were employed in this study. Two magnitudes of ground motions with their root mean square (RMS) accelerations equal to 0.03g and 0.05g respectively were produced by the shaking table. During the tests, the standalone frame without TMD and the frame with EMTMD connected with different circuits were tested individually, and consequently the control and energy harvesting performance of the EMTMD was evaluated.

Energy harvesting circuit

The AC voltage output of the three-phase rotary EM damper needs to be converted to DC output by a three-phase bridge rectifier comprising six Schottky diodes (Figure 3(a)). Figure 3(b) shows a simplified model of the structure equipped with the EMTMD, in which the EM damper and the three-phase bridge rectifier are represented by a two-port model which connected with a full-wave bridge rectifier; and the pendulum-type EMTMD is represented by a linear-motion EMTMD. In this two-port model, C_p stands for the parasitic damping coefficient accounting for various mechanical losses such as friction losses, magnetic losses, etc.; T_{em} is the EM damping torque; F_{em} is the EM damping force; R_{coil} and L_{coil} are the equivalent resistance and inductance of the coil of the EM device ($R_{coil}=2R$; $L_{coil}=2L$). According to Faraday's law of induction, and assuming the pendulum-type EMTMD with minor swing, we have

$$u_0 = K_{em}\omega \approx K_{em}\dot{z}\,n_g / l, \quad i_0 = T_{em} / K_{em} \approx F_{em}\,l / n_g K_{em}, \tag{1}$$

where, u_0 is the electromotive force (emf), i_0 is the current in the coil, K_{em} is machine constant of the rotary EM damper, ω is the angular velocity of the rotor in the EM damper (in rad/s), $\dot{z}$ is the linear velocity of EMTMD relative to the primary structure, n_g is the gear box ratio of the three-phase rotary EM device, l is length of the pendulum, F_{em} is equivalent EM damping force of

EMTMD. K_{em} was identified as 0.7921 V.s/rad from the experimental u_0/ω ratio. The coil resistance, R_{coil} is equal to 2R, which value is 34.0Ω. Two different circuits, namely Circuit A and Circuit B, were connected to the EMTMD and tested in this study:

Circuits A – A single resistor was connected to the rectifier, representing a general electrical load with constant resistance [Figure. 3(b)]. Due to the low frequency feature of the primary structure and the relative small value of L_{coil} of the EM damper, the effect of the coil inductance is ignorable in this experimental study. According to the widely accepted impedance-matching principle [9, 14, 30], the external resistance R_{load} was tuned to be equal to the internal resistance, namely, 34 Ω. This case is designed to assess the potential energy harvesting capability by the EMTMD system under impedance-matching condition.

Circuit B –In order to maintain a stable charge voltage of the Li-ions battery, a DC-DC converter was employed to regulate the random output voltage from the EMTMD. Because the EMTMD in real-scale civil structures is expected be much greater than those in conventional harvesters, its output voltage will be much higher than the voltage of rechargeable batteries, and consequently, a buck or buck-boost converter needs to be used in most applications. A non-isolated buck-boost converter (LDOC03-005W05-VJ) shown in Figure 3(b) is selected in this experiment. The switching buck-boost converter adjusts the duty cycles according to the changing output voltage via a fixed-frequency pulse-width-modulator (switching frequency: 1.5MHz). The allowed input voltage of LDOC03 is 3-13.8V, and the output voltage is tuned to 4.2V, a standard charge voltage for Li-ion batteries. The capacitance of input capacitor C_{in} is 15.4mF.

Power flow

Figure 4 indicates the power flow of the SVCM system, from the dynamic excitations to the ultimate power consumption by WSS. The average excitation power to the structure-EMTMD system can be computed by:

$$P_{ex} = -\frac{1}{t_2 - t_1}\int_{t_1}^{t_2} m_s \ddot{x}_g(t)[\dot{x}_g(t) + \dot{y}_s(t)]dt - \frac{1}{t_2 - t_1}\int_{t_1}^{t_2} m_{tmd} \ddot{x}_g(t)[\dot{x}_g(t) + \dot{y}_{tmd}(t)]dt \quad (2)$$

where m_s and m_{tmd} are, respectively, the mass of the primary structure and the EMTMD; $\ddot{x}_g(t)$ is the acceleration of ground motion; $\dot{y}_s(t)$ and $\dot{y}_{tmd}(t)$ are, respectively, the linear velocity of the primary structure and the EMTMD relative to the ground. As the mass ratio of TMD, i.e. m_{tmd}/m_s, is typically small, the second term in Equation (2) is often ignorable. The excitation power P_{ex} is converted to three additive parts, i.e., the inherent damping power of the structure P_{ds}, the rate of change (ROC) of structural vibration energy P_{vs} and the absorbed power by the EMTMD P_{tmd},

$$P_{ex} = P_{ds} + P_{vs} + P_{tmd} \quad (3)$$

The power absorption of the EMTMD would effectively suppress the vibration of the primary structure. The power absorbed by the EMTMD is further converted into the ROC of vibration energy of the EMTMD P_{vt} and the damping power of the EMTMD P_{in},

$$P_{tmd} = P_{vt} + P_{in} \tag{4}$$

The second term P_{in} is essentially the input power to the EM damper and the energy harvesting system.

If we assume the structure behaves elastically, the vibration energy consists of the kinetic energy and the elastic potential energy, and thus the ROC of vibration energy of the structure and the EMTMD are given by

$$P_{vs} = \frac{E_{vs}(t_2) - E_{vs}(t_1)}{t_2 - t_1} = \frac{\frac{1}{2}m_s\dot{y}_s^2(t_2) + \frac{1}{2}k_s y_s^2(t_2) - \frac{1}{2}m_s\dot{y}_s^2(t_1) - \frac{1}{2}k_s y_s^2(t_1)}{t_2 - t_1} \tag{5}$$

$$P_{vt} = \frac{E_{vt}(t_2) - E_{vt}(t_1)}{t_2 - t_1} = \frac{\frac{1}{2}m_{tmd}\dot{y}_{tmd}^2(t_2) + \frac{1}{2}k_{tmd} y_{tmd}^2(t_2) - \frac{1}{2}m_{tmd}\dot{y}_{tmd}^2(t_1) - \frac{1}{2}k_{tmd} y_{tmd}^2(t_1)}{t_2 - t_1} \tag{6}$$

When the system is subjected to a stationary excitation, the change of vibration energy would be small and the average ROC over a long period would be minimal and ignorable. Consequently, the average excitation power P_{ex} is approximately equal to the summation of the damping powers of the structure and the EMTMD, and the average absorbed power by the EMTMD is approximately equal to the damping power of the EMTMD, given that the structure and the EMTMD remains entirely elastic. The average dissipated power by structural inherent damping can be estimated by

$$P_{sd} = \frac{1}{t_2 - t_1}\int_{t_1}^{t_2} C_s \cdot \dot{y}_s^2(t)dt \tag{7}$$

where C_s is the inherent damping coefficient. Unlike conventional TMDs in which the damping power is just dissipated, the damping power in the EMTMD becomes the input power P_{in} to the electromagnetic damping and energy-harvesting (EMDEH) subsystem, which consists of the EM damper and the external circuit [Figure 3(b)].The EMDEH subsystem is the main component of the SVCM system, and the input power can be further separated to several additive terms:

$$P_{in} = P_p + P_{em} = P_p + P_{coil} + P_g = P_p + P_{coil} + P_{ehc} + P_{out} \tag{8}$$

where, P_p is the average parasitic damping power; P_{em} is the average EM damping power that is the power converted to the electric domain by electromagnetic induction; P_{coil} is average power of copper loss; P_g is the average gross output power from the EM damper, P_{ehc} is the average power loss of the EHC, P_{out} is the average output power. As mentioned before, if the swing of the pendulum is small, the pendulum-type TMD can be simplified as a linear oscillator in horizontal direction. The average parasitic damping power P_p can be estimated by

$$P_p = \frac{1}{t_2 - t_1}\int_{t_1}^{t_2} C_p \cdot \dot{z}^2(t)dt \tag{9}$$

where C_p is the parasitic damping coefficients of the EMTMD. $\dot{z}(t) = \dot{y}_{tmd} - \dot{y}_s$ is the linear velocity of EMTMD relative to the primary structure. The average copper loss P_{coil} is calculated by

$$P_{coil} = \frac{1}{t_2 - t_1}\int_{t_1}^{t_2} i_1^2(t)R_{coil}dt = I_{1,rms}^2 R_{coil} \tag{10}$$

where i_1 and $I_{1,rms}$ are, respectively, the transient and RMS current flowing in the coils of the EM device; R_{coil} is the resistance of the coil. The average gross output power P_g and the average net output power P_{out} from the EM device in a general EHC (e.g. Circuit B) are

$$P_g = \frac{1}{t_2 - t_1}\int_{t_1}^{t_2} u_1(t) \cdot i_1(t)dt \tag{11}$$

$$P_{out} = \frac{1}{t_2 - t_1}\int_{t_1}^{t_2} u_2(t) \cdot i_2(t)dt \tag{12}$$

where u_1 is the transient input voltage to the EHC; u_2 and i_2 are respectively the voltage and charging current of the rechargeable battery (as shown in Figure 3(b)). The overall energy conversion efficiency η of the EMDEH subsystem (or SVCM system) is defined as

$$\eta = \frac{P_{out}}{P_{in}} = \eta_1 \cdot \eta_2 \cdot \eta_3 \tag{13}$$

where η_1, η_2 and η_3 are three intermediate energy conversion coefficients defined as

$$\eta_1 = \frac{P_{em}}{P_{in}}, \qquad \eta_2 = \frac{P_g}{P_{em}}, \qquad \eta_3 = \frac{P_{out}}{P_g} \tag{14}$$

η_1 is the electromechanical coupling coefficient that describes the conversion efficiency from the total damping power of the EMTMD to electrical power, and the power loss due to the parasitic damping should be minimized in order to enhance the efficiency η_1. η_2 stands for the efficiency of the EM damper, which is affected by the power loss due to the coil resistance. η_3 is the efficiency of the EHC, and a low power consumption of the DC-DC converter is always desired.

Particularly in Circuit A, there is no power consumption by the EHC,

$$P_g = P_{out} = \frac{U_{rms}^2}{R_{load}} \tag{15}$$

The energy conversion coefficients are

$$\eta_1 = \frac{C_{em}}{C_p + C_{em}} = \frac{\xi_{em}}{\xi_p + \xi_{em}} = \frac{\xi_{em}}{\xi_d}, \qquad \eta_2 = \frac{R_{load}}{R_{load} + R_{coil}}, \qquad \eta_3 = 1 \tag{16}$$

Circuit A is one of the simplest representative EHCs for assessing the capability of energy harvesting [14]. As it does not involve any power loss in the external circuit, it is a good reference to assess the efficiency of the EHC when the system is subjected to the same excitation.

TESTING RESULTS

This section discusses the testing results, with respect to the control effect, energy harvesting efficiency and functionality of the WSS.

A. Control effects

Figure 5 shows the FFT spectra of the free vibration displacement of the frames without and with the EMTMD system respectively. The EMTMD is connected to Circuit A. Similarly to other TMDs, the regenerative EMTMD also adds one more DOF to the primary structure. As a result, two dominant frequencies can be observed in the FFT spectrum after the installation of the EMTMD. The considerably reduced peaks imply the enhanced damping of the structure due to the EMTMD.

Figure 6 shows the FRFs of structural displacement responses due to ground motions (RMS ground accelerations of 0.03 g and 0.05g) for the structures without control and with the EMTMD (Circuit A and Circuit B). Similar to the displacement spectra in Figure 5, two dominant peaks can be seen in Figure 6 for the controlled structures with the EMTMD. The peak magnitudes of the structural FRFs have been considerably reduced by around 10dB in the displacement responses as well as in the acceleration responses. The almost overlapping FRFs reveal that the control effects of the EMTMDs connected to Circuit A or Circuit B are very close, with a slightly better control effects under a larger excitation condition (0.05g). The damping ratios of the structures were estimated based on the displacement responses under the random ground motions and their values are also shown in Table 2. It should be noted that both the parasitic damping and EM damping are theoretically dependent on the vibration amplitude. The nonlinearity of the parasitic damping is mainly contributed by the friction; whereas the nonlinearity in the EM damping is due to the varying impedance of the EHC when the EMTMD is connected with Circuit B. For example, the EM damping is nearly zero and the parasitic damping is considerable if the vibration amplitude is small. Such nonlinear damping characteristics were also reported and discussed by [23]. Therefore, the estimated damping ratios are the equivalent values under the random excitation. However, only slight difference in the control performance can be observed at the two excitation magnitudes.

Figure 7 indicates that the displacement and acceleration responses under random ground motions for the uncontrolled structure, and the structures with Circuit A and Circuit B. It is observed that the structure responses are effectively suppressed by the EMTMD when connected with either Circuit A or Circuit B. The control effect in the case of Circuit B is still close to the case of Circuit A. Table 2 presents more detailed

comparison of the control performance under the random ground motions with the RMS accelerations equal to 0.03 g. The peak displacement $y_{s,max}$, the peak acceleration $\ddot{y}_{s,max}$, the RMS displacement $y_{s,rms}$, and the RMS acceleration $\ddot{y}_{s,rms}$ are summarized in the table. A significant reduction can be achieved in both the displacement and acceleration responses. The comparisons clearly indicate that the case of Circuit B has a comparably good control effect as Circuit A. Therefore, the aforementioned nonlinearity involved in Circuit B did not deteriorate the control performance in this experiment.

B. Energy harvesting efficiency

Circuit A

Figure 8 shows the time histories of the output voltage (the voltage on R_{load}) for Circuit A when the structure is subjected to a random ground motion of RMS 0.03g. The output voltage is a stochastic process, and its peak value is up to 8.664V in Figure 8. In general, a larger TMD mass, a smaller friction loss in the bearing, gear box and EM damper, or a larger motion of the TMD will lead to a higher voltage output. It should be pointed out that the mass of TMD in real civil structures is huge in comparison with those in conventional EM energy harvesters, and consequently the output voltage and power will be considerably greater than those for other small EM energy-harvesting devices whose output voltages are typically hundreds of mV [31].

Given the output voltage, the output power in Circuit A can be estimated using Equation (15). Figure 9(a) shows the variation of the output power during the shaking table test, as well as the EM damping power P_{em}, the input power to the EMTMD P_{in}, and the excitation power from the ground motion to the structure. As revealed by Equation (3) and (4), the difference between the excitation power and the total damping power is equal to the ROC of the vibration energy of the entire system. Meanwhile, the output power varies during the shaking table test, which implies that the output power is dependent on the magnitude of the ground excitation. The average output power of the electric load is 200.9mW. Other average powers in the power flow are presented in Table 3. Figure 9(b) shows the variation of the efficiencies over time, in which, the electromechanical coupling coefficient η_1 varies from 41.8% to 53.1%. The energy conversion efficiency η can be computed according to Equation (13). It ranges from 20.9 % to 26.6%, with the average value equal to 24.1%. Since no power loss occurs in the Circuit A, the energy conversion efficiency η shows the same variation trend as the electromechanical coupling coefficient η_1. In addition, the variation of the power of EMTMD when connected to Circuit A under the ground motion level of 0.05g is presented in Figure 9(c). With the increase of ground motion magnitude, the peak output voltage of EMTMD grows to 17.1V and the output power of this case is 930.3 mW. It is found that the output power is proportional to the cubic magnitude of the random ground motions. Furthermore, the parasitic damping of EMTMD consists of two parts, friction damping and viscous damping, which values are shown in Table 1. Therefore, the equivalent parasitic damping coefficient or ratio will become smaller with increasing the motion amplitude of the EMTMD, and which will result in a higher electromechanical coupling coefficient η_1, as shown in Figure 9(d). As the increasing of the electromechanical coupling coefficient η_1, a higher energy conversion efficiency, 33.6% was measured in this case, which is close to the value estimated by Equation (16).

Circuit B

This section presents the power efficiency of the regenerative EMTMD connected with Circuit B under random excitations. Circuit B represents a real EHC. In Circuit B, the DC-DC converter is always associated with power loss, and the actual impedance of the circuit varies under random excitations. As a result, the energy conversion efficiency of Circuit B is observed to be less than that in Circuit A which does not involve any power loss in the circuit.

Figure 10 shows the performance of the buck-boost converter. Figure 10(a) shows the input and output voltage of the buck-boost converter without connecting to the battery or any electric load under a random ground motion of RMS 0.05g. Though the input voltage shows a substantial fluctuation, the DC-DC converter could maintain a stable output voltage of 4.2V on the battery, with minimal ripples observed. Figure 10(b) presents the case in which the EHC is connected to a Li-ion battery, and a stable output voltage u_2 of 3.8V can be maintained. It should be noted that the input voltage higher than 10V is beyond the measurement range, and the actual fluctuation in the input voltage is greater than observed in Figure 10.

Figure 11 indicates that the time histories of the battery voltage and the charging current during the shaking table tests, when Circuit B is connected to a Li-ion battery. Under the random ground motion of 0.05g, the voltage of the rechargeable battery slightly increases over time as can be seen in Figure 11(a), and it implies that the Li-ion battery can be successfully charged by the EHC and store the energy from the regenerative EMTMD. Figure 11(b) shows the output current from the rectifier i_1 and the charging current i_2 in the battery. An apparently nonlinear relationship between u_1 and i_1 has been observed during the test, and thus the transient impedance of the circuit is not constant in this case. As the EM damping force is proportional to the current in the coil, i.e. the current output from the rectifier i_1, the EM damping coefficient varies under the random vibrations. The average charge current is around 18.7 mA and 81.3 mA under random ground motions of 0.03g and 0.05g, respectively. According to Equations (11) and (12) , the power P_g and P_{out} can be calculated using the measured voltage and current. Figure 12 shows the variation of different powers under the ground motion of 0.05g. Different types of power show similar fluctuation trend in Figure 12(a). In general, they become greater with the increase of the excitation magnitude. Table 3 presents more power terms in this case. It can be seen that around 65.6%~92% of the total excitation energy is "consumed" by the regenerative EMTMD in this experimental study, which justifies its good vibration control performance. Figure 12(b) shows the variation of energy conversion coefficients in this case. By comparing Figure 9(d) and Figure 12(b), it is seen that the electromechanical coupling coefficient η_1 is approximately close between two cases – Circuit A and Circuit B under the same ground motion level. Though the energy conversion coefficient η_2 remains stable during the test, the corresponding average value of 40.6% is lower than that for Circuit A, which implies that the equivalent impedance of Circuit B under the ground motion of 0.05g is around 23 Ω (according to Equation 16. The average gross output power from the EM damper is around 735.6 mW, less than that of Circuit A. The final output power to the battery, however, dramatically drops to 312.4 mW, representing a low efficiency of the DC-DC converter (η_3=43.1%). It should be noted that the nominal efficiency of the buck-boost converter is above 90%. In this study, the input power or current is much lower than the optimal range of the DC-DC converter, and results in a relatively low

efficiency. Such a low efficiency can be further improved by selecting a suitable DC-DC converter. The energy conversion coefficients η_1 and η_2 are 67.1% and 40.6% respectively. The overall energy conversion efficiency is around 11.7%. The average powers in other testing scenarios are summarized in Table 3. For example, the average energy conversion coefficient η_2 and the gross output power P_g under the ground motion of 0.03g are, respectively, equal to 48.3% and 193.6 mW, both close to those in Circuit A. It implies that the equivalent impedance of Circuit B under the ground motion of 0.03g is very close to the impedance-matching condition, although the transient impedance is not constant. The increase of the excitation magnitude produces a higher emf, and it corresponds to a relatively lower equivalent impedance of the EHC in the experiments.

C. Power Wireless Sensor

The Li-ion battery which is charged by the Circuit B connected to the EMTMD is used to power the Imote2 wireless sensor with SHM-A sensor board. As aforementioned, its power consumption is about 204 mW in standby state and 626 mW in sensing state according to the measured data in this experiment. As shown in Table 3, the average output power is 68.9 mW and 312.4mW respectively under the ground motions of 0.03g and 0.05g. Therefore, the EMTMD-powered wireless sensing is only conducted under the ground motion of 0.05g. The time histories of the battery voltage, output power and the power consumption of WSS are shown in Figure 13. The Li-ion battery is charged in the first sixty seconds; the voltage drops slightly during 60-80 sec, as the output power is less than the standby power of Imote2; the peak power consumption occurs between 84.7 to 113.5 second when the power consumption of WSS was boosted up from the standby state to the sensing state, and the Li-ion battery is discharged as evidenced by the clear voltage drop. It should be pointed out that (1) most WSS are not intended for continuous structural monitoring in practical applications, and thus the average power consumption in long run should be considerable lower than its peak power. For example, the average power consumption of the Imote2 in this experiment is around 299 mW, still slightly less than the average output power of the EMTMD; (2) the output power of full-scale EMTMD in real buildings or structures would be greater by several orders of magnitude, surely sufficient as power supplies to WSS. In addition, the performance of the WSS was validated through the comparison of wireless and wired sensing signals. Figure 14 shows the horizontal acceleration response between 98.3 to 108.54 second collected by the Imote2 WSS and the conventional wired accelerometer. The sampling frequency of the both system is equal to 100 Hz, and thus totally 1024 sensing data were collected. A good agreement between the wired and wireless sensing data exhibits the WSS collected high-quality acceleration data during the test. More high frequency components can be observed in the wireless data, simply because of different low pass filter used instead of noise. At the sampling frequency of 100 Hz, the cut-off frequency of the low pass analog filter is 40 Hz in the WSS, which is four times that of the wired sensing system. It should be noted that the whole sensing process of the WSS consists of setup, data sensing, data resample, and data transmission. Therefore, the duration of the peak power consumption (shown in Figure 13) is always longer than that of the acceleration data (shown in Figure 14). In summary, the experimental results of this study clearly verify the feasibility of the proposed self-powered vibration control and monitoring system, consisting of a regenerative EMTMD, an EHC and a WSS.

CONCLUSIONS

This paper proposes a novel self-powered vibration control and monitoring (SVCM) system, an integration of a regenerative EMTMD and a WSS. The regenerative EMTMD, composed of a pendulum-type TMD, an EM damper and an EHC, provides both vibration damping and energy harvesting functions. Proof-of-concept tests of a single-story frame equipped with the SVCM system were performed on a shaking table. Experimental results under random ground motions illustrate that the EMTMD can effectively suppress the structural vibration and successfully power a commercial WSS that monitor the dynamic response of the structure. The performance of structural control, energy harvesting and vibration monitoring is assessed individually for the tested SVCM system. The structural responses (the displacement and acceleration) were considerably reduced by 49.6-65.8% under the control of the EMTMD with a mass ratio of 3.33%. The signal collected by the WSS can well represent the acceleration response of the frame. Under the ground motion levels of 0.03g and 0.05g (RMS), the average output power is 200.9 mW and 930.3 mW respectively for Circuit A, and 68.9 mW and 339.9 mW respectively for Circuit B. Slightly nonlinear behavior in the damping, control performance and energy harvesting efficiency could be noted by comparing the experimental results under the two ground motions levels. Its impact needs to be quantitatively characterized in future by more numerical and experimental study. It may complicate the optimal solution of the EMTMD, and should be paid enough attention in the design methodology.

The output power and voltage of the EMTMD in this experimental study is much higher than those of small or micro electromagnetic harvesters reported in the literature, because of its relatively larger mass. The output power is generally proportional to the mass of the energy-harvesting oscillator. Considering the huge mass of full-scale EMTMDs in real civil structures, their actual output power will be even greater than the values reported in this study by orders of magnitude, and be sufficient to power a number of sensors. The output power is certainly dependent on the excitation magnitude. Therefore, the proposed new strategy is especially appealing to the situations in which control and sensing is required only when excessive vibration happens.

The energy efficiency found in this experimental study is not high, compared with the theoretical upper limit. The reduction of the power loss due to the parasitic damping and EHC can further improve the energy conversion efficiency of the system. It needs to be investigated in future. However, the experimental results still demonstrate a great potential to implement this novel SVCM system in real civil or mechanical structures. The regenerative power produced by the EMTMD will be valuable in some emergency or hazardous situations.

ACKNOWLEDGEMENT

The authors are grateful for the financial support from the Research Grants Council of Hong Kong through a

GRF grant (Project No. 533011) and from the Hong Kong Polytechnic University through a Niche Area Program (Project No. 1-BB6X). Findings and opinions expressed here, however, are those of the authors alone, not necessarily the views of the sponsor.

REFERENCES

[1] J.P. Lynch, K.J. Loh, A summary review of wireless sensors and sensor networks for structural health monitoring, Shock and Vibration Digest, 38 (2006) 91-128.

[2] G. Park, T. Rosing, M.D. Todd, C.R. Farrar, W. Hodgkiss, Energy harvesting for structural health monitoring sensor networks, J. Infrastruct. Syst., 14 (2008) 64-79.

[3] R. Bogue, Wireless sensors: A review of technologies, products and applications, Sens. Rev., 30 (2010) 285-289.

[4] P. Glynne-Jones, M.J. Tudor, S.P. Beeby, N.M. White, An electromagnetic, vibration-powered generator for intelligent sensor systems, Sens. Actuator A-Phys., 110 (2004) 344-349.

[5] S.P. Beeby, R.N. Torah, M.J. Tudor, P. Glynne-Jones, T. O'Donnell, C.R. Saha, S. Roy, A micro electromagnetic generator for vibration energy harvesting, J. Micromech. Microeng., 17 (2007) 1257-1265.

[6] R. Torah, P. Glynne-Jones, M. Tudor, T. O'Donnell, S. Roy, S. Beeby, Self-powered autonomous wireless sensor node using vibration energy harvesting, Meas. Sci. Technol., 19 (2008).

[7] J.H. Cho, R.F. Richards, D.F. Bahr, C.D. Richards, M.J. Anderson, Efficiency of energy conversion by piezoelectrics, Appl. Phys. Lett., 89 (2006).

[8] S.R. Anton, H.A. Sodano, A review of power harvesting using piezoelectric materials (2003-2006), Smart Mater. Struct., 16 (2007) R1-R21.

[9] S. Wang, K.H. Lam, C.L. Sun, K.W. Kwok, H.L.W. Chan, M.S. Guo, X.Z. Zhao, Energy harvesting with piezoelectric drum transducer, Appl. Phys. Lett., 90 (2007).

[10] S.C. Stanton, A. Erturk, B.P. Mann, D.J. Inman, Nonlinear piezoelectricity in electroelastic energy harvesters: Modeling and experimental identification, J. Appl. Phys., 108 (2010).

[11] P.D. Mitcheson, P. Miao, B.H. Stark, E.M. Yeatman, A.S. Holmes, T.C. Green, MEMS electrostatic micropower generator for low frequency operation, Sens. Actuator A-Phys., 115 (2004) 523-529.

[12] R. Kornbluh, R. Pelrine, Q. Pei, R. Heydt, S. Stanford, S. Oh, J. Eckerle, Electroelastomers: Applications of dielectric elastomer transducers for actuation, generation and smart structures, in: A.M.R. McGowan (Ed.), San Diego, CA, 2002, pp. 254-270.

[13] P.D. Mitcheson, Analysis and Optimisation of Energy-Harvesting Micro-Generator Systems, in, Imperial College London, London,UK., 2005.

[14] S. Priya, Modeling of electric energy harvesting using piezoelectric windmill, Appl. Phys. Lett., 87 (2005) 1-3.

[15] T.T. Soong, G.F. Dargush, Passive energy dissipation system in structural engineering, John Wiley & Sons Ltd., Chichester, UK, 1997.

[16] G.W. Housner, L.A. Bergman, T.K. Caughey, A.G. Chassiakos, R.O. Claus, S.F. Masri, R.E. Skelton, T.T. Soong, B.F. Spencer, J.T.P. Yao, Structural control: Past, present, and future, J. Eng. Mech.-ASCE, 123 (1997) 897-971.

[17] T.T. Soong, B.F. Spencer Jr, Supplemental energy dissipation: State-of-the-art and state-of-the-practice, Eng. Struct., 24 (2002) 243-259.

[18] Y.L. Xu, K.C.S. Kwok, B. Samali, The effect of tuned mass dampers and liquid dampers on cross-wind response of tall/slender structures, J. Wind Eng. Ind. Aerodyn., 40 (1992) 33-54.

[19] I. Kourakis, Structural systems and tuned mass dampers of super-tall buildings: case study of Taipei 101, in: Department of Civil and Environmental Engineering, Massachusetts Institute of Technology, USA, 2005.

[20] R. Palomera-Arias, J.J. Connor, J.A. Ochsendorf, Feasibility study of passive electromagnetic damping systems, J. Struct. Eng.-ASCE, 134 (2008) 164-170.

[21] R. Palomera-Arias, Passive Electromagnetic Damping Device for Motion Control of Building Structures, in: Department of Architecture, Massachusetts Institute of Technology, 2005, pp. 146.

[22] W.A. Shen, S. Zhu, Y.L. Xu, Modeling of linear electromagnetic damper for vibration control and energy harvesting, in: the 12th East Asia-Pacific Conference on Structural Engineering and Construction (EASEC-12), Hong Kong, 2011.

[23] S. Zhu, W.A. Shen, Y.L. Xu, Linear electromagnetic devices for vibration damping and energy harvesting: Modeling and testing, Eng. Struct., 34 (2011) 198-212.

[24] S. Priya, D.J. Inman, Energy harvesting technologies, Spinger Science Business Media, LLC., New York, USA, 2009.

[25]Crossbow Technology, Imote2 Hardware Reference Manual, in, http://www.xbow.com/Support/Support_pdf_files/Imote2_Hardware_Reference_Manual.pdf., 2007.

[26] J.A. Rice, K.A. Mechitov, S.H. Sim, B.F. Spencer Jr, G.A. Agha, Enabling framework for structural health monitoring using smart sensors, Structural Control and Health Monitoring, 18 (2011) 574-587.

[27] J.A. Rice, B.F. Spencer, Flexible smart Sensor Framework for Autonomous Full-scale Structural Health Monitoring, in: NSEL Report Series, University of Illinois at Urbana-Champaign, 2009.

[28] J.A. Rice, K. Mechitov, S.H. Sim, T. Nagayama, S. Jang, R. Kim, B.F. Spencer Jr, G. Agha, Y. Fujino, Flexible smart sensor framework for autonomous structural health monitoring, Smart. Struct. Syst., 6 (2010) 423-438.

[29] G. Litak, M.I. Friswell, S. Adhikari, Magnetopiezoelastic energy harvesting driven by random excitations, Appl. Phys. Lett., 96 (2010).

[30] A.R. Hambley, Electrical Engineering Principles and Applications, Fifth ed., Pearson, 2011.

[31] R. Dayal, S. Dwari, L. Parsa, A new design for vibration-based electromagnetic energy harvesting systems using coil inductance of microgenerator, IEEE Trans. Ind. Appl., 47 (2011) 820-830.

Table 1. Properties of frame and pendulum-type EMTMD

Steel Frame without TMD		Pendulum-type EMTMD	
Height of frame, h (m)	1.636	Length of pendulum, l (mm)	186
Mass of frame, m_s (kg)	527.9	Mass of TMD, m (kg)	17.6
Width b_1 (m)	1.04	Mass ratio of EMTMD, μ (%)	3.3
Width b_2 (m)	0.65	Frequency of EMTMD*, f_{tmd}(Hz)	1.06
Frequency of frame, f_s (Hz)	1.078	Frequency ratio of EMTMD, α	0.99
Damping of frame, ξ_s (%)	0.95	Constant Parasitic Torque (N.m)	0.6
		Parasitic damping coefficient (N.m.s/rad)	0.01
		Parasitic damping of EMTMD, ξ_p (%)	3.8
		EM damping of EMTMD*, ξ_{em} (%)	6.3
		Total Damping of EMTMD*, ξ_d (%)	10.1

* measured when EMTMD was connected with Circuit A (Angle: 17^0).

Table 2. Control effects of EMTMD (ground acceleration: RMS 0.03g)

Scenarios	RMS Responses		Peak Responses		Damping Ratio
	$\ddot{y}_{s,rms}$ (m/s^2)	$y_{s,rms}$ (mm)	$\ddot{y}_{s,\max}$ (m/s^2)	$y_{s,max}$$(mm)$	(%)
Without control	0.941	20.155	3.446	69.842	0.95
With EM-TMD (Circuit A)	0.365	8.207	1.081	24.230	4.22
Reduction (%)	61.21	59.28	68.63	65.33	----
With EM-TMD (Circuit B)	0.322	8.310	1.466	35.17	4.59
Reduction (%)	65.78	58.77	57.46	49.64	----

Table 3. Power and efficiency

Circuit	$\ddot{x}_g$	P_{ex} (mW)	P_{in} (mW)	P_p (mW)	P_{em} (mW)	P_g (mW)	P_{out} (mW)	η_1 (%)	η_2 (%)	η_3 (%)	η (%)
A	0.03g	1015.5	821.2	419.4	401.8	200.9	200.9	48.9	50	100	24.5
A	0.05g	4072.2	2715.5	854.9	1860.6	930.3	930.3	67.2	50	100	33.6
B	0.03g	890.3	818.7	418.0	400.7	193.6	68.9	48.9	48.3	35.6	8.4
B	0.05g	4130.8	2709.7	892.7	1817	735.6	312.4	67.1	40.6	43.1	11.7
B*	0.05g	3654	2613.1	1030	1583.1	646.2	339.9	60.6	40.8	52.6	13

*connected with WSS

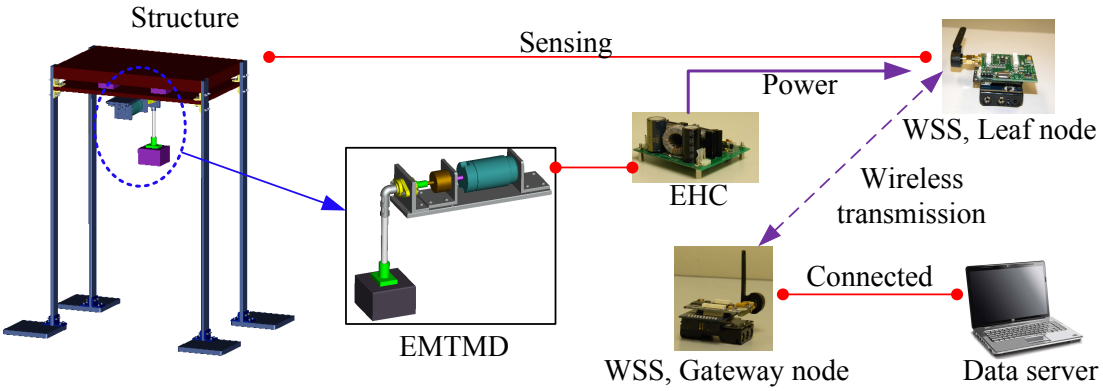

Figure 1. Configuration of SVCM system with regenerative EMTMD and WSS

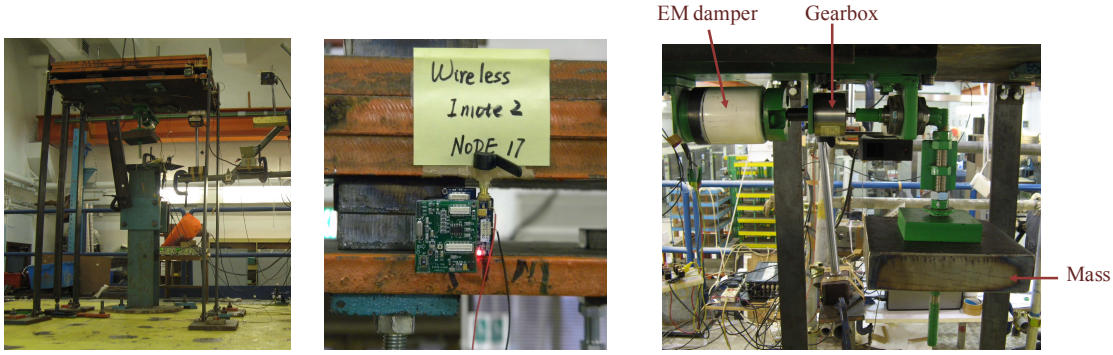

(a) SDOF model (b) Imote2 WSS (c) EMTMD

Figure 2 Shaking table experimental setup

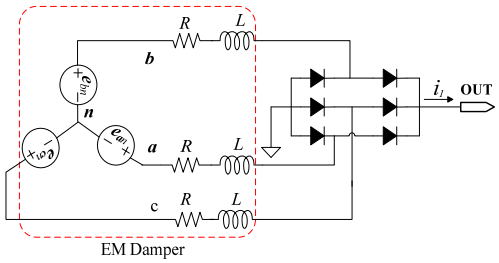

(a) Three-phase rotary EM damper connected with a three-phase bridge rectifier

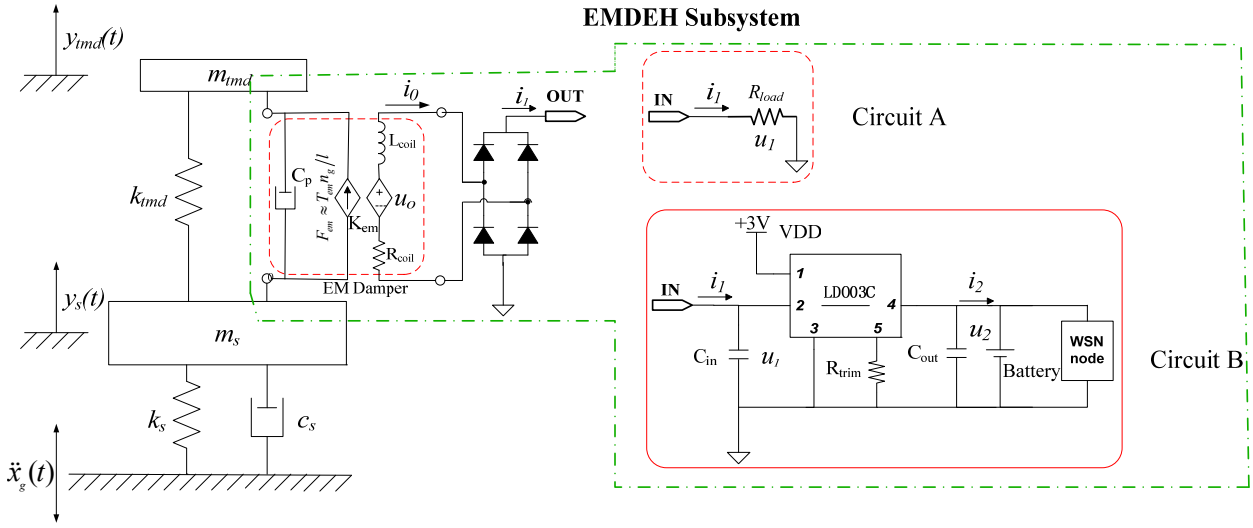

(b) Simplified Model of the EMTMD and EHC (Circuit A and Circuit B)

Figure 3. Simplified model of EMTMD and its EHCs

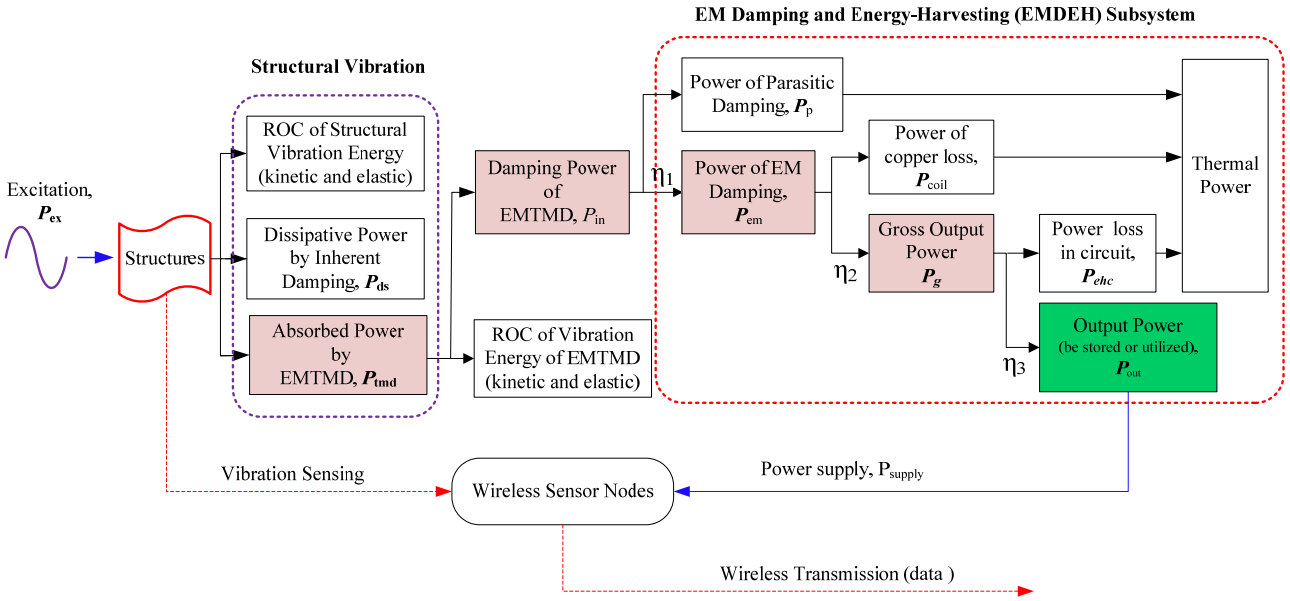

Figure 4. Power flow of a structure with an electromagnetic SVCM system

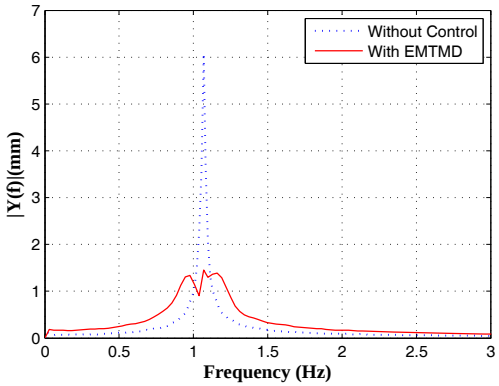

Figure 5 FFT spectra of displacement responses of the primary structures without and with EMTMD (Circuit A)

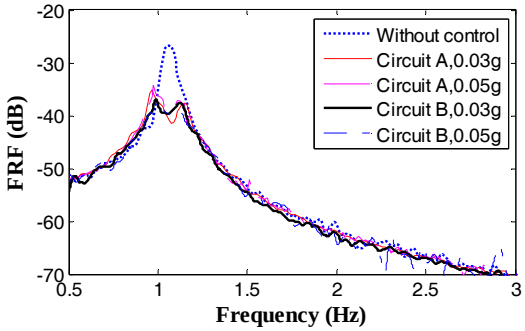

Figure 6. FRFs of displacement responses of the primary structures with and without EMTMD (Ground motion level of 0.03g and 0.05g)

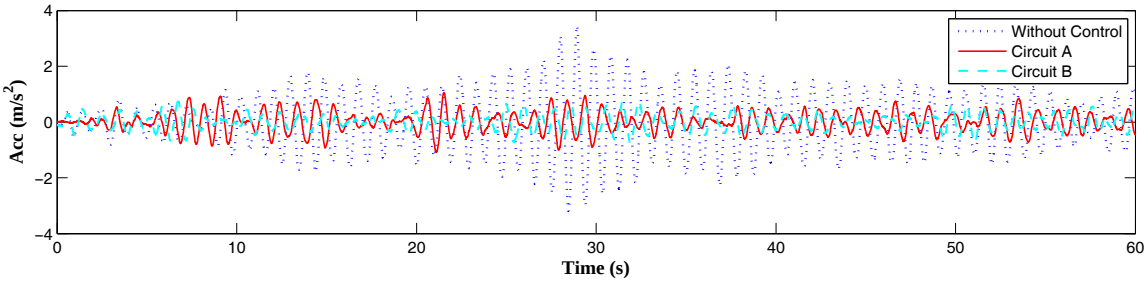

(a) Structural acceleration responses

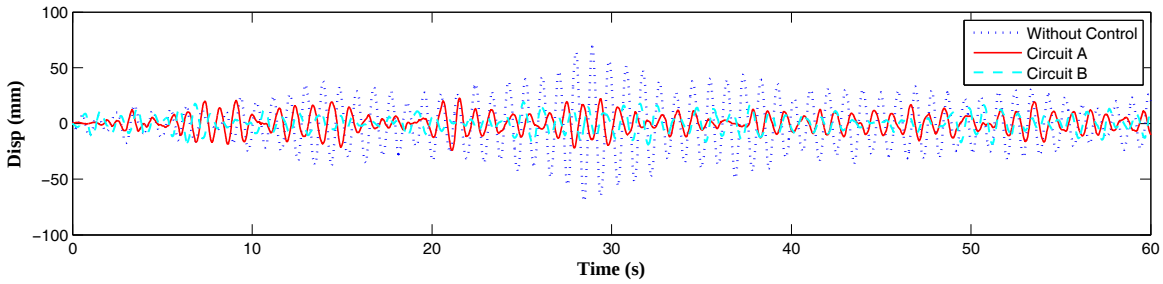

(b) Structural displacement responses

Figure 7 Comparisons of structural response time histories without control and with EMTMD(Ground acceleration: RMS 0.03 g).

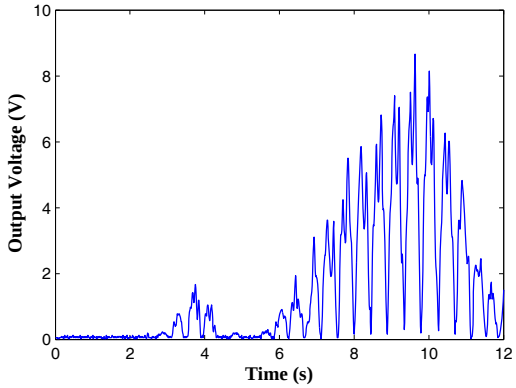

Figure 8 Time history of output voltage (Circuit A)

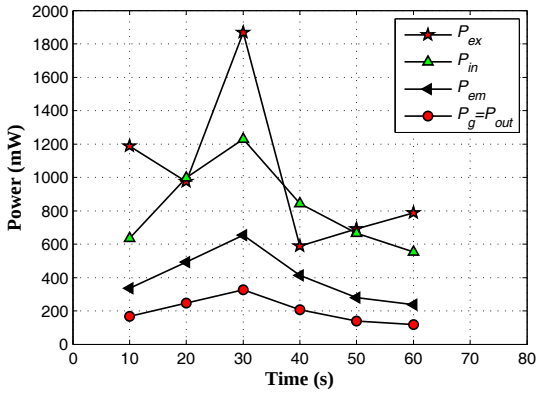

(a) variation of power over time (0.03g)

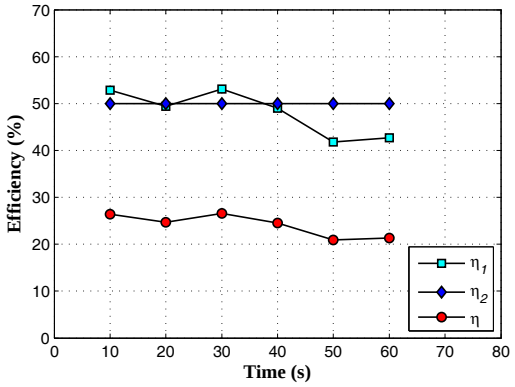

(b) variation of efficiency over time (0.03g)

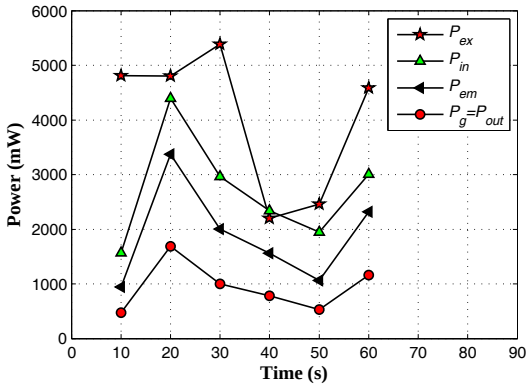

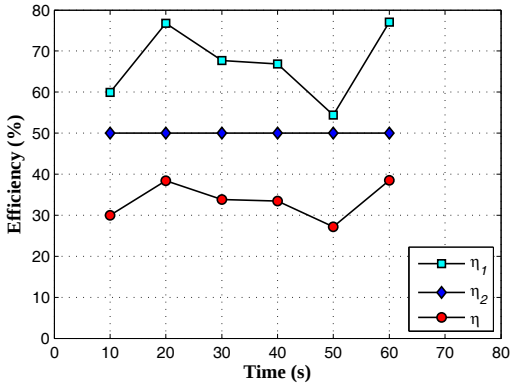

(c) variation of power over time (0.05g) (d) variation of efficiency over time(0.05g)

Figure 9 Energy harvesting performance for Circuit A during shaking table test

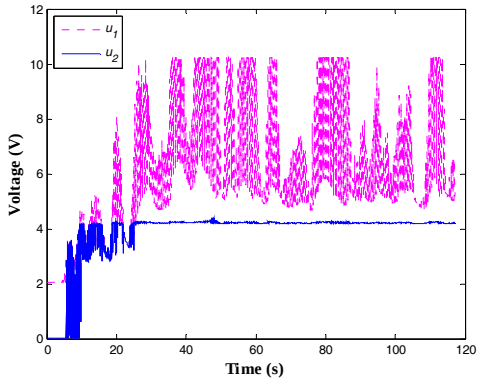

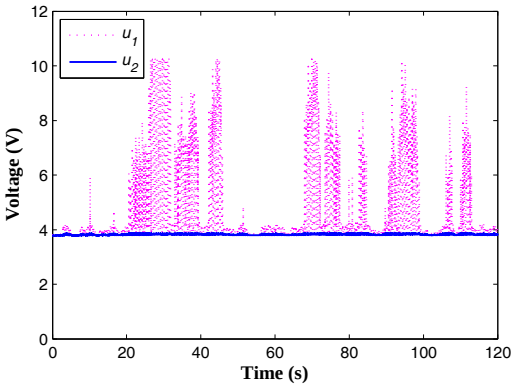

(a) without electric load (b) charging Li-ion battery

Figure 10 Input and output voltages of the DC-DC converter of circuit B (Ground acceleration: RMS 0.05 g)

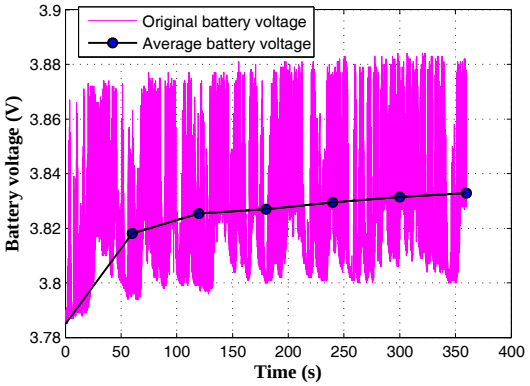

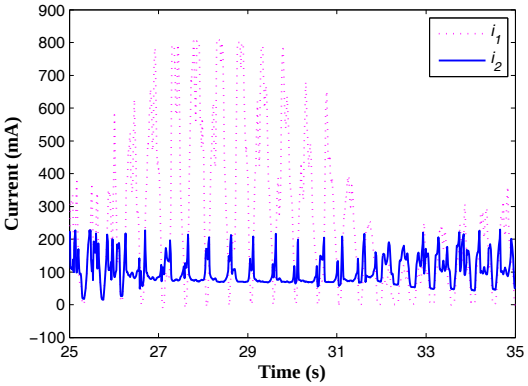

(a) battery charging curve (b) input current and charging current

Figure 11 Charging voltage and current to Li-ion battery (Circuit B, Ground acceleration: RMS 0.05 g)

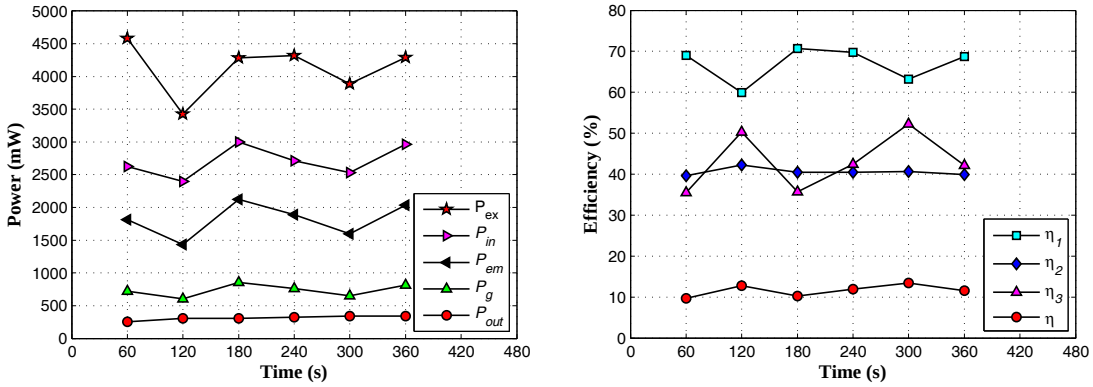

(a) variation of power over time (b) variation of efficincy over time

Figure 12 Power and efficiency of regenerative EMTMD system (Circuit B, Ground acceleration: RMS 0.05 g)

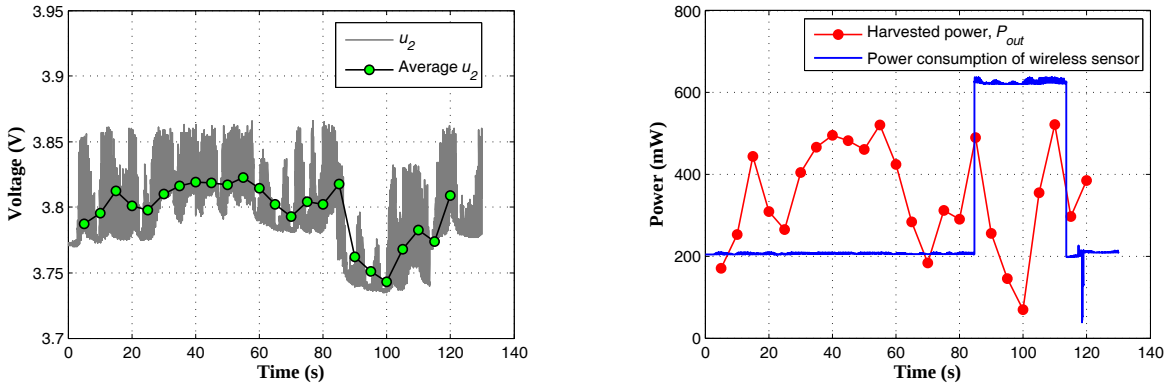

(a) battery voltage time history (b) variation of power

Figure 13 Variation of battery voltage and output power (Circuit B connected with WSS, Ground acceleration: RMS 0.05 g).

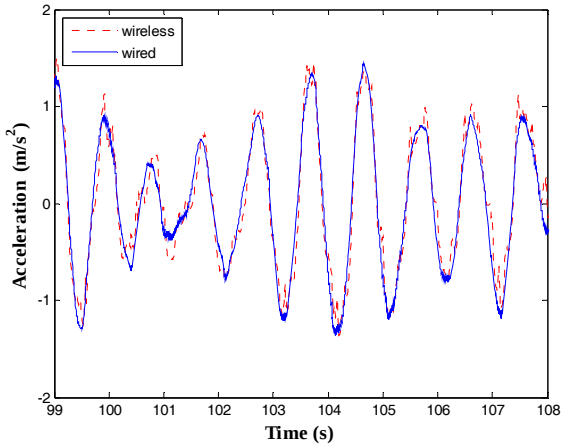

Figure 14 Comparison of wireless and wired acceleration signals of primary structure